# Addition of Al_20_3 to the Al_20_3/AC // Si Electrode to Enhance the Performance of Supercapattery

Diantoro, Markus
Department of Physics, Faculty of Mathematics and Natural Sciences, State University of Malang

Nasikhudin
Department of Physics, Faculty of Mathematics and Natural Sciences, State University of Malang

Suryana, Risa
Department of Physics, Faculty of Mathematics and Natural Sciences, Sebelas Maret University

Ade Siyanti Nurul Hidayah
Department of Physics, Faculty of Mathematics and Natural Sciences, State University of Malang

他

https://doi.org/10.5109/7236853

出版情報：Evergreen. 11 (3), pp.2081-2090, 2024-09. Interdisciplinary Graduate School of Engineering Sciences, Kyushu University, Japan
バージョン：

# Addition of $Al_2O_3$ to the $Al_2O_3$/AC // Si Electrode to Enhance the Performance of Supercapattery

Markus Diantoro[1,2,*], Nasikhudin[1,2], Risa Suryana[3], Ade Siyanti Nurul Hidayah[1], Nadea Catur Nurmayanti[1], Worawat Meevasana[4]

[1]Department of Physics, Faculty of Mathematics and Natural Sciences, State University of Malang, Jl. Semarang 5, Malang 65145, Indonesia

[2]Center of Advanced Materials for Renewable Energy (CAMRY), State University of Malang, Jl. Semarang 5, Malang 65145, Indonesia

[3]Department of Physics, Faculty of Mathematics and Natural Sciences, Sebelas Maret University, Jl. Ir. Sutami 36A Kentingen Surakarta 57126 Indonesia

[4]Department of Physics, Faculty of Science, Suranaree University of Technology, Nakhon Ratchasima 111, Thailand

*Author to whom correspondence should be addressed:
E-mail: markus.diantoro.fmipa@um.ac.id

(Received October 30, 2023: Revised May 15, 2024: Accepted June 21, 2024).

**Abstract**: Supercapattery has the potential to optimize energy and power densities. The availability of silicon and carbon may be one of our concerns. This research is focused on developing anodes based on silicon with 10% $Al_2O_3$/AC as a cathode. The electrodes were synthesized using the blending method. The XRD analysis showed diffraction peaks indicating the activated carbon and silicon phases. The absorption functional groups were identified through FTIR characterization. SEM analysis showed that the increasing mass of $Al_2O_3$ caused the porosity to increase. The combination of 10% $Al_2O_3$/AC//Si/CB supercapattery devices offers superior performance with a specific capacitance of 105.8 $Fg^{-1}$, an energy density of 46.3 $Whkg^{-1}$, and a power density of 336.7 $Wkg^{-1}$.

Keywords: supercapattery; $Al_2O_3$; activated carbon; silicon; nickel-foam; renewable energy

## 1. Introduction

Energy is a grave sector because its availability has a supporting role for all activities of human civilization[1]. The augmentative of the worldwide energy crisis is caused by the scarcity of fossil fuels, global warming, pollution, and environmental degradation, which has encouraged the perfection of energy storage technologies with high and stable performance, low production cost, environmentally friendly, and sustainable[2–4]. The development of energy storage media is one solution to deal with these problems[5,6]. Lithium-ion batteries (LIBs) are one of the energy storage media used in portable electronic devices and vehicles[7]. Lithium-ion batteries are one of the best energy storage systems compared to batteries based on lead-acid materials[8]. LIBs also have advantages such as high electrochemical performance, high energy density, good cyclic ability, and low possibility of self-discharge[9]. However, the battery has the disadvantage of a voltage drop when it is used in the long term and has high cycles. The new breakthrough of energy storage media is a supercapacitor, high-power energy storage based on charge discharge at the electrode or electrolyte interface surface through electrostatic phenomena or electrochemical ion adsorption. Supercapacitor devices are categorized into carbon-based EDLCs and pseudocapacitors based on metal oxide and polymer material[10]. LIBs and batteries are proficient for storing large amounts of energy (high energy density). In comparison, supercapacitors have a higher power density, which gives faster charge and discharge energy (high power density) through Faradaic reactions[11,12]. Although the performance of supercapacitors and LIBs is quite good, there is still a need to develop hybrid devices that combine the advantages of supercapacitors and batteries called supercapattery[13–15].

In the last decade, the development of supercapattery has become the focus of research in energy storage. Supercapattery is a hybrid type of supercapacitor, and battery components combine both advantages[16]. Supercapacitors can store power in the long term (long lifetime), have high power density, are environmentally friendly, and have low energy density[17]. Meanwhile, the battery has a high energy density of around 150-200 Wh/kg[18–20]. Therefore, the combination of supercapacitors and batteries has excellent potential to make an efficient energy storage appliance with high energy and power density[21,22]. Ion accessibility performance and surface modification in energy storage devices significantly improve supercapattery performance[23,24].

The supercapattery device is arranged by several essential components, including the positive side electrode (cathode), negative side electrode (anode), electrolyte, and a separator as a barrier between the electrodes to prevent contact[25]. The performance of the supercapattery device is determined by the material of electrode[26]. Therefore, anodes with high specific capacitance are needed to optimize the performance of supercapattery devices. Si is paid much attention among all battery component storage materials because of its very high theoretical intercalation capacity and superior low operating voltage, abundant presence, and environmentally friendly24 (. These advantages cause Si-based anodes to have high capacitance and energy density[27]. Based on research conducted by Jiarong He, et al. (2022), the electrochemical performance of Si-anode has a specific capacitance of 1502.1 $mAhg^{-1}$ with retention of 51.1% for 105 cycles[28]. However, Si-based anodes have the disadvantages of significant volume changes and low conductivity, leading to a rapid decline in capacitance performance and poor cycle stability[29,30]. Various strategies are proposed to overcome this problem, such as combining Si material with conductive materials such as carbon and its derivatives. Another solution is to use polymer binders to improve the stability of the electrode structure and hydrogen bond interactions on Si-based electrodes[31].

The application of metal oxides as supercapacitor electrode materials is an exciting topic because of their low cost, environmental friendliness, and abundance in nature[32]. In addition, metal oxide-based electrodes have high capacitance characteristics through redox reactions. Based on research conducted by Diantoro et al., it has successfully synthesized supercapacitor electrodes based on the metal oxide $SrTiO_3$ with a specific capacitance of 5.433 F/g[33]. Another oxide material used as a supercapacitor electrode is Al2O3 or alumina, which has high thermal conductivity and corrosion resistance. Although the electrical conductivity is lower than other metal oxides, $Al_2O_3$ has excellent chemical stability and a large specific surface area[34]. $Al_2O_3$/AC composite-based supercapacitor electrodes have a semicrystalline phase with a smaller surface area than ordinary activated carbon-based electrodes. Research by Azizi et al. (2020) and Liu et al. (2020) showed the synthesized of asymmetric supercapacitor with electrodes based on reduced graphene oxide/polyindole (rGO/Pln)/gama- $Al_2O_3$/AC and $Al_2O_3$/AC nanowire polyvinyl butyral (NW-PVB). The specific capacitance results in both studies were 308 and 146 F/g[35,36].

In addition to metal oxides, another material that excels as a constituent of supercapacitor electrodes is activated carbon, with a high surface area, good mechanical strength, and low production cost[37]. Activated carbon is affordable, accessible from various carbon-rich biomass, easy to synthesize, and can be obtained in various forms such as powders, fibers, and composites[38]. Activated carbon is effectively used as a supercapacitor's main ingredient because it has good cycle stability, high conductivity, and extended performance life[39]. The high conductivity of activated carbon can reduce the resistance level of the supercapacitor so that the resulting performance is higher. Research related to the $Al_2O_3$ cathode-based supercapattery combined with the Li-ion anode previously showed a specific capacitance that was less than optimum[40]. We present the effect of the addition of $Al_2O_3$ on its morphology, structure, crystal size, functional group, porosity, and electrochemical performance of $Al_2O_3$/AC and Si/Carbon black. The electrochemical performance of the supercapattery is described as specific capacitance, energy, and power density.

## 2. Experimental

### 2.1 Materials

Materials used to synthesize supercapacitor electrodes include $Al_2O_3$ powder from Sigma Aldrich, Germany, activated carbon, carbon black, acrylonitrile multi-copolymer (LA133) binder from Redox, Sweden, and deionized water (OneMed 99%). Meanwhile, synthesizing Si electrodes as battery components uses Merck's Si nanoparticle powder, polyvinylidene fluoride (PVDF) from Merck., and dimethylacetamide (DMAC). The organic electrolyte used in this experiment is tetraethylammonium tetrafluoroborate (Et4NBf4) with acetonitrile solvent, and the separator is cloth fiber type.

### 2.2 Instrumental and Analysis Method

The microstructural characterization was carried out through X-ray diffractometer (XRD) PAN Analytical EXPERT-3, Fourier Transform Infra-Red (FT-IR), and Scanning Electron Microscope (SEM) FEI INSPECT-S50 type instruments. XRD characterization was used to determine the diffraction peak, degree of crystallinity, structure, phase, and the size of the electrode crystal formed. In XRD characterization, the Cu-Kα wave has a wavelength of 1.54060 Å with a diffraction angle range between 10-90° .The crystal size is determined using the Scherrer equation, which can be written in Equation (1).

$$D = \frac{K\lambda}{\beta cos\theta} \quad (1)$$ [41]

D defined crystal size, K is the Scherrer constant (0.89), $\lambda$ is the wavelength (0.1546 nm), $\beta$ is the FWHM, and

$\theta$ is the Bragg angle. The degree of crystallinity is determined by Equation 2.

$$crystallinity: \frac{crystaline\ fraction}{(crystalline+amorphus\ fraction)} x\ 100\% \quad (2)$$

FTIR characterization was used to determine the functional groups contained, with a wavenumber range of 500 – 4000 $cm^{-1}$. SEM characterization was used to identify particle size, porosity, and pore diameter.

Meanwhile, the characterization of the electrochemical performance of the supercapattery device was tested using the Galvanostatic Charge-Discharge "Battery Testing System NEWARE" 5V 6A. Based on the resulting charge-discharge graphic analysis, it can be processed to determine specific capacitance, energy density, and power density using the following equations.

$$C_s = \frac{4I}{\Delta V/\Delta t} \quad (3)$$ [42]

$$ED = 0.5C(\Delta V)^2 \quad (4)$$ [43]

$$PD = \left(\frac{ED}{\Delta t}\right) x\ 3600 \quad (5)$$ [44]

### 2.3 Procedure

#### 2.3.1 Synthesis of $Al_2O_3$/AC/CB Electrode on Al-foil

We used raw materials to synthesize supercapacitor electrodes, including $Al_2O_3$ powder, activated carbon, carbon black, LA133 binder, and deionized water. About 2 g of active electrode material has been prepared with a ratio of 1:0.1:0.9 for binders, conductive materials, and active ingredients. The synthesis process was started by dissolving 1 g of LA133 binder in 2.5 mL of deionized water on a hotplate at 100 rpm for 30 minutes at room temperature. After the binder dissolved and no air bubbles, 0.1 g of carbon black powder was added, and the rotation speed was increased to 150 rpm. After all the black carbon is dispersed, then 0.9 g of the active materials in the form of $Al_2O_3$ and activated carbon are added gradually with a predetermined composition of 5% and 10% $Al_2O_3$. After all the ingredients were homogeneous, the solution was stirred at 300 rpm for 24 hours to produce a paste. The paste was then deposited using a doctor blade on an aluminum foil substrate with a thickness of 20 µm. This electrode was subsequently heated in an automatic oven at room temperature for 30 minutes, then at 60°C for 30 minutes, 30 minutes at 80°C, and 100°C in one hour. This gradually increased heating process is carried out so that the electrode is not damaged due to thermal shock.

#### 2.3.2 Synthesis of Si/CB Electrode on Nickel-foam

The synthesis of Si/CB electrodes as battery components uses Si nanoparticle powder, carbon black, polyvinylidene fluoride (PVDF), and dimethylacetamide (DMAC). The electrodes were prepared using a total mass of 0.5 g with a ratio of 1:1:3 for binders, conductive materials, and active ingredients. The synthesis process was started by dissolving 0.1 g of PVDF into 4 mL of DMAC using a hotplate at 200 rpm for 1 hour at 80°C. After the PVDF dissolved, the solvent temperature was reduced to room temperature while the speed was increased to 300 rpm. Then, gradually add 0.1 g of carbon black. After the carbon black dispersed, we added 0.3 g of Si and stirred until homogeneous. After all the ingredients were mixed, the solution was stirred for 7 hours. This solution was deposited on a thin disk nickel-foam substrate with a diameter of 1.5 cm, and the initial mass was weighed. About 20 µL of the solution was deposited using a micropipette on both sides of the substrate. The electrodes were then heated in an oven at 80°C for an hour. If the sample was dry, the mass was weighed, and the sample was diluted using a press with a load of 500 kg. After that, the electrodes were immersed in Et4NBf4 1.0 M electrolyte for 24 hours. This immersion process was carried out so that the pores could maximally absorb the electrolyte solution on the nickel-foam substrate. The electrolyte was prepared by dissolving 2.17 g Et4NBf4 into 10 mL of acetonitrile.

#### 2.3.3 Fabrication of Coin Cells Device

The two types of electrodes are fabricated into coin cells using a cloth fiber separator with the arrangement shown in Fig. 1. This fabrication process was divided into 3 types of arrangement at the cathode and anode. First, the symmetric $Al_2O_3$/AC electrode was fabricated on the cathode and anode as supercapacitor side. Second, the symmetry Si/CB electrode is fabricated on the cathode and anode as battery side. Third, fabrication of 10% $Al_2O_3$/AC as cathode and Si/CB as anode for supercapattery device arrangement.

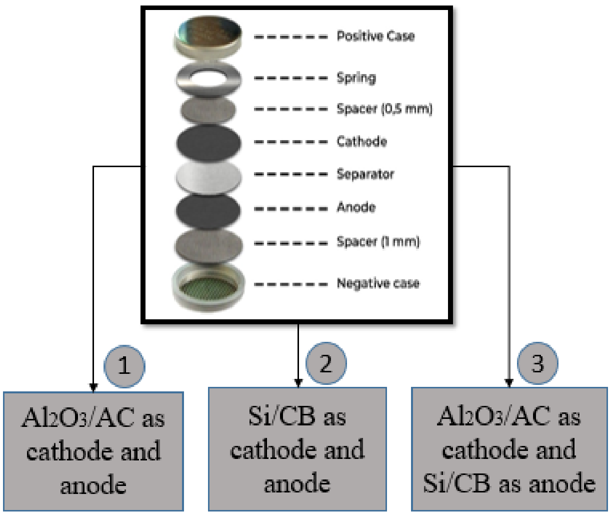


**Fig. 1:** Coin cell arrangement.

## 3. Result and Discussion

### 3.1 X-Ray Diffraction (XRD) Analysis

The X-ray diffraction of AC/CB, $Al_2O_3$/AC electrode with compositions of 5% and 10% is shown in Fig. 2. An amorphous arrangement showing activated carbon's structure dominates the diffraction pattern formed. The diffraction peaks of activated carbon are shown at angles of 2θ = 26.50° and 43.36° with the crystal planes of (002) and (100)[45,46]. In addition to the diffraction peak of activated carbon, at an angle of 2θ = 38.47° with the (111) plane, it shows the diffraction peak of the aluminum foil substrate used[47]. No diffraction peaks of $Al_2O_3$ were observed in the electrode samples with 5 and 10% $Al_2O_3$ due to its smaller amount and ratio than activated carbon as a composite.

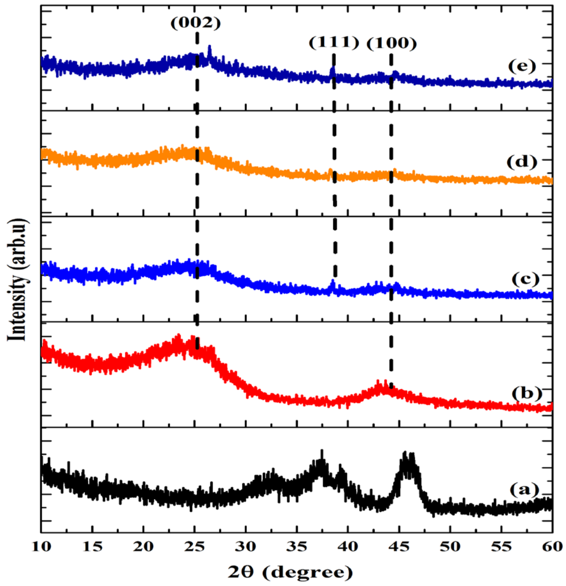


**Fig. 2:** XRD pattern of (a) raw $Al_2O_3$, (b) raw AC, (c) AC/CB/Al-foil, (d) 5% $Al_2O_3$/AC/CB/Al-foil, and (e) 10% $Al_2O_3$/AC/CB/Al-foil.

Figure 3 compares the diffraction patterns of Si powder and Si/CB electrode. The diffraction patterns observed at (111), (220), (311), and (400) planes with angles of 2θ = 28.4°, 47.3°, 56.1° and 69.1° (JCPDS No. 27 – 1402)[48,49]. Compared to Si nanoparticles, the diffraction pattern of Si/CB electrode has a lower intensity. The low intensity represents the amount of diffracted materials, which is also low. Another peak at 2θ = 65.1° was identified as the peak of the aluminum foil substrate used during characterization.

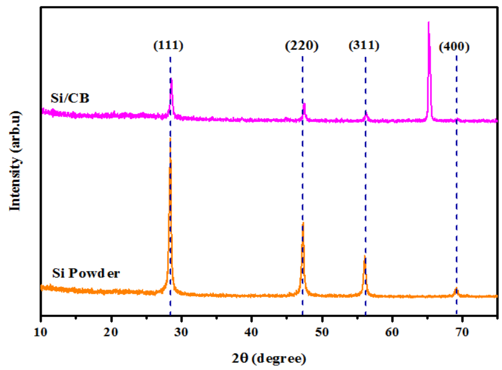


**Fig. 3:** XRD pattern of Si powder and Si/CB electrode.

From the diffraction pattern of Fig. 3, we can obtain crystal phase, crystallite size, and degree of crystallinity. Crystallite size and degree of crystallinity can be observed in Table 1. The crystallite size of the Si nanoparticles is 50.0 nm, comparable to the research conducted by Zhang et al. (2020)[49]. Meanwhile the crystallite size and crystallinity of Si/CB electrode is 33.5 nm and 26.7 %, subsequently. Crystallite size and crystallinity could affect the redox reactions and conductivity increase. The relatively low crystallinity due to the amorphous structure of carbon black addition can provide more electroactive surfaces for redox reactions and better diffusion of electrolyte ions due to structural defects and irregular atomic arrangement.

Table 1. Crystallite size and degree of crystallinity of Si powder and Si/CB electrode.

| Sample | Crystallite size(nm) | Crystallinity(%) |
|---|---|---|
| Si | 33.5 | 26.7 |
| Si Powder | 50.0 | 50.4 |

### 3.2 Functional groups analysis

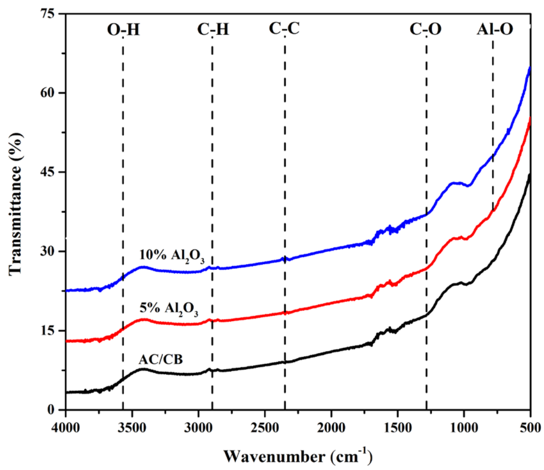


**Fig. 4:** FTIR spectra of AC/CB/Al-foil, 5% $Al_2O_3$/AC/CB/Al-foil, and 10% $Al_2O_3$/AC/CB/Al-foil.

FTIR characterization was used to ensure the absorption functional groups from the thin film of supercapacitor electrodes based on AC/CB/Al-foil, 5% $Al_2O_3$/AC/CB/Al-foil, and 10% $Al_2O_3$/AC/CB/Al-foil presented in Fig. 4. Wave number 3529.73 $cm^{-1}$ shows an O-H (hydroxyl) absorption functional group[50)]. At a peak at a wave number of 2889.37 $cm^{-1}$, there is a functional group with C-H absorption ([51)]. Wave number 2380.16 indicates the presence of a C-C absorption functional group[52)]. Wave number 1288.45 cm-1 shows the functional group from C-O, and 781 $cm^{-1}$ indicates the absorption functional group from Al-O[53,54)].

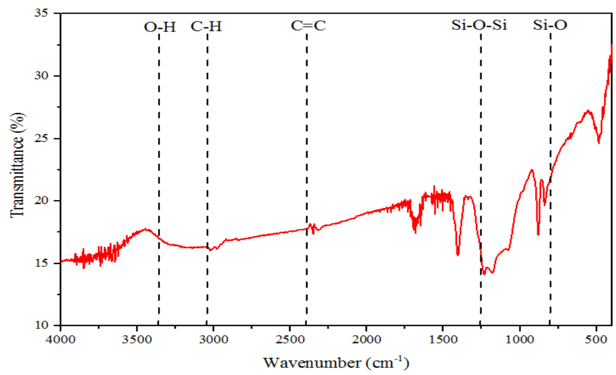


**Fig. 5:** FTIR spectra of Si/CB electrode.

Figure 5 shows an absorption functional group contained in a thin film of Si/CB-based battery electrodes. At wave number 3371.57 $cm^{-1}$ there is a functional group group from O-H absorption[55)]. At the wave number of 3022.45 $cm^{-1}$ there is an absorption functional group C-H[56)]. A peak at 2351.23 $cm^{-1}$ indicates the presence of an absorption functional group C=C[57)]. Wave number 1141 $cm^{-1}$ shows the functional group of Si-O-Si, and 775.38 $cm^{-1}$ declares the existence of the absorption functional group from Si-O[58,59)].

### 3.3 Morphology and porosity analysis

SEM is an equipment used to determine the morphology and topology of a material. In addition, the SEM characterization shows the porosity of the electrodes, which affects the electrochemical performance. The surface morphology of Si powder is shown in Fig. 6, while the AC/CB/Al-foil, 5% $Al_2O_3$/AC/CB/Al-foil, 10% $Al_2O_3$/AC/CB/Al-foil, and Si/CB electrodes are presented in Fig. 7.

The analysis shows that the average particle size of Si powder is 60.0 nm, with the histogram distribution as shown in Fig.6. The results of the Si particle size are based on the research of Tian et al. (2019), which suggests that the distribution of Si particles ranges from 20.0 – 60.0 nm[60)]. Fig. 7 (a) shows that the activated carbon from AC/CB/Al-foil electrode has a morphology resembling a sheet lump and large pores. Figures 7 (b) and (c) show the 5% and 10% A12O3/AC/CB/Al-foil electrode morphology. From the figure, it shows that the morphology of electrode dominated with activated carbon morphology. This result also linear with XRD analysis in the previous section. Figure 7 (d) shows the morphology of the Si/CB electrode deposited on a nickel-foam substrate. This image shows the porous nickel-foam substrate with a pore diameter of 4.352 nm. The substrate used shows large pores, which aid the maximum absorption of electrolyte ions.

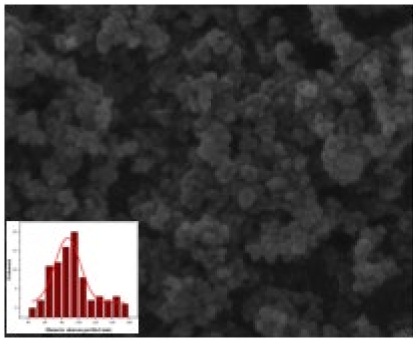

**Fig. 6:** The morphology of Si powder and its hystogram of particle distribution size.

Porosity obtained from Fig.7 electrodes shown in Table 2. Porosity the space between the materials that functions to absorb ions from the electrolyte. Porosity analysis shows that as the mass of $Al_2O_3$ used increases, the porosity will also increase.

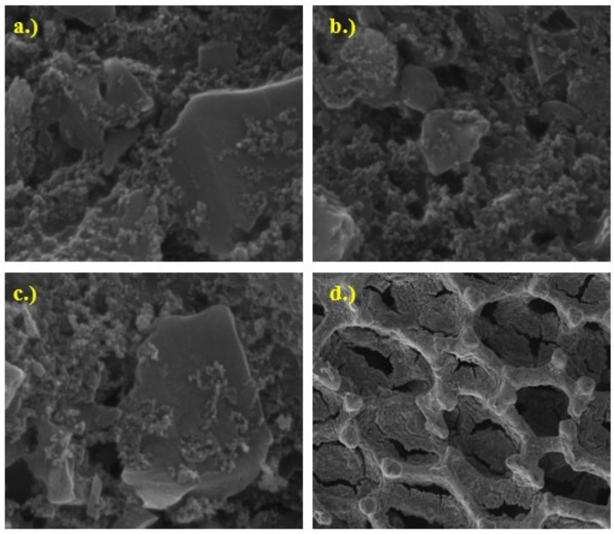


**Fig. 7:** SEM of (a) AC/CB, (b) 5% $Al_2O_3$/AC/CB, (c) 10% $Al_2O_3$/AC/CB, and (d) Si/CB electrodes.

Table 2. The porosity of supercapattery electrodes.

| **Electrodes** | **Porosity (%)** |
|---|---|
| AC/CB | 64.4 |
| 5% $Al_2O_3$/AC/CB | 66.3 |
| 10% $Al_2O_3$/AC/CB | 69.1 |
| Si/CB | 75.4 |

### 3.4 Electrochemical performance analysis

The electrochemical performance characterization of the symmetrical coin cell 5% $Al_2O_3$/AC/CB, 10% $Al_2O_3$/AC/CB, Si/CB/Nickel-foam, and asymmetric 10% $Al_2O_3$/AC//Si/CB-based supercapattery was identified through the Galvanostatic Charge-Discharge (GCD) instrument. Figure 8 shows the results of charge-discharge using 1.0 M organic liquid electrolyte Et4NBf4. Based on the resulting charge-discharge graphic analysis, it can be processed to determine specific capacitance, energy density, and power density using the equation (3), (4), and (5).

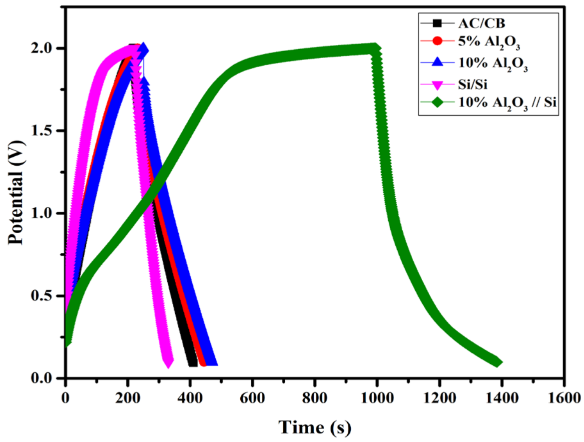


**Fig. 8:** Galvanostatic Charge-Discharge graph for symmetric AC/CB, 5% $Al_2O_3$/AC/CB, 10% $Al_2O_3$/AC/CB, Si/CB, and asymmetric 10% $Al_2O_3$/AC/CB // Si/CB in coin cell devices.

Cs is the specific capacitance ($Fg^{-1}$), I is the discharge current in units of mA, t is the discharge time (s), and V is the potential difference (V). The other parameters, m, denote the electrode mass (mg), ED is the energy density ($Whkg^{-1}$), and PD is the power density ($Wkg^{-1}$). Figure 8 shows a voltage vs. time of one cycle of each coin cell. The results of electrochemichal performance is presented in Table 3.

It is found that adding $Al_2O_3$ in a symmetric supercapacitor increases specific capacitance, energy density, and power density. Adding $Al_2O_3$ increases the surface area and porosity and provides more electroactive surfaces for faradaic redox reactions to increase performance. The Si/CB charge-discharge graph shows a low specific capacitance of 24.6 $Fg^{-1}$. This specific capacitance is due to the nature of the Si material, which is less stable, so it has low retention during the process of charge discharge.

Table 3. Specific capacitance, energy density, and power density for symmetric AC/CB, 5% $Al_2O_3$/AC/CB, 10% $Al_2O_3$/AC/CB, Si/CB, and asymmetric 10% $Al_2O_3$/AC/CB //Si/CB in coin cell devices.

| Electrodes | Cs ($Fg^{-1}$) | ED ($Whkg^{-1}$) | PD ($Wkg^{-1}$) |
|---|---|---|---|
| AC/CB | 34.5 | 10.7 | 297.9 |
| 5% $Al_2O_3$/ AC/CB | 43.8 | 15.9 | 307.1 |
| 10% $Al_2O_3$/ AC/CB | 50.1 | 17.9 | 331.0 |
| Si/CB | 24.6 | 10.7 | 313.5 |
| 10% $Al_2O_3$/ AC/CB// Si/CB | 105.8 | 46.3 | 336.7 |

The combination of the two components in the form of a supercapattery based on a 10% $Al_2O_3$/AC/CB cathode and a Si/CB anode yields excellent electrochemical performance with a specific capacitance of 105.8 $Fg^{-1}$, an energy density of 46.3 $Whkg^{-1}$, and a power density of 336.7 $Wkg^{-1}$. The supercapattery sample shows a cyclical shape representing the components between the supercapacitor and the battery. This GCD shape is similar to that of activated carbon-based EDLC supercapacitors. This analysis's results align with the research conducted by Chen et al. (2020)[61]. Furthermore, this study shows a higher specific capacitance than the $Al_2O_3$-based supercapattery with Li-ion anode conducted by Ndipingwi et al. (2018)[40].

## 4. Conclusion

From XRD analysis showed that activated carbon's structure dominates the diffraction pattern of 5% and 10% $Al_2O_3$/AC/CB electrodes. The diffraction peaks of activated carbon are shown at angles of $2\theta = 26.50°$ and 43.36° with the crystal planes of (002) and (100). Si powder showed a crystallite size of 50.0 nm with crystallinity of 50.4%, meanwhile Si/CB electrode had crytallite size of 26.7 with the crystallinity of 26.7%. FTIR analysis of the AC/CB, 5% and $Al_2O_3$/AC/CB electrode showed the presence of functional groups O-H hydroxyl, C-H, C-C, C-O, and Al-O at wave numbers between 3529.73 – 781 $cm^{-1}$. The Si/CB electrode showed the functional groups O-H, C-H, C=C, Si-O-Si, and Si-O at wave numbers between 3371.57 – 775.38 $cm^{-1}$. SEM analysis on Si powder showed its particle distribution of 60.0 nm. The porosity of the electrode increased, and reach the optimum point of 69.1 % at 10% $Al_2O_3$ addition. Si/CB electrode on nickel-foam substrate has a porosity of 75.4%. From GCD analysis showed that the symmetric coin cell device of 10% $Al_2O_3$/AC have optimum electrochemical performance, such as 50.1 $Fg^{-1}$ for specific capacitance, 17.9 $Whkg^{-1}$ for energy density, and 331.0 $Wkg^{-1}$ for power density. Symmetric coin cell device of Si/CB electrode showed specific capacitance of 24.6 $Fg^{-1}$, energy density of 10.7 $Whkg^{-1}$, and power density of 313.5 $Wkg^{-1}$. The supercapattery device of 10% $Al_2O_3$/AC // Si showed good performance with a specific capacitance of 105.8 $Fg^{-1}$, an energy density of 46.3 $Whkg^{-1}$, and a power density of 336.7 $Wkg^{-1}$.

## Acknowledgements

This work was funded through the Internal UM 2022 research grant under the Kerjasama Internasional scheme with the contract number 19.5.934/UN32.20.1/LT/2022 lead by Prof. Dr. Markus Diantoro, M.Si.

## Nomenclature

| | |
|---|---|
| D | crystal size (nm) |
| $C_S$ | specific capacitance ($Fg^{-1}$) |
| *PD* | power density ($Wkg^{-1}$) |
| ED | energy density ($Whkg^{-1}$) |
| *V* | voltage (V) |
| t | time |

*Greek symbols*

| | |
|---|---|
| $\lambda$ | wavelength (nm) |
| $\beta$ | FWHM (–) |
| $\theta$ | Bragg angle (degree) |
| $\kappa$ | Scherrer constant |

## References


1) Anisa Raditya Nurohmah, Cornelius Satria Yudha, Mintarsih Rahmawati, Shofirul Sholikhatun Nisa, Arif Jumari, Hendri Widiyandari, and Agus Purwanto, "Structural and electrochemical analysis of iron doping in lini_0.6-x mn_0.2 co_0.2 fe_x o_2 battery," *Evergreen*, **8** (*1*) 82–88 (2021). doi:10.5109/4372263.
2) A.A. Hor, N. Yadav, and S.A. Hashmi, "High energy density carbon supercapacitor with ionic liquid-based gel polymer electrolyte: role of redox-additive potassium iodide," *Journal of Energy Storage*, **47** 103608 (2022). doi:10.1016/j.est.2021.103608.
3) Y. Zhao, H. Hao, T. Song, X. Wang, C. Li, and W. Li, "High energy-power density zn-ion hybrid supercapacitors with n/p co-doped graphene cathode," *Journal of Power Sources*, **521** 230941 (2022). doi:10.1016/j.jpowsour.2021.230941.
4) M. Bansal, A. Agarwal, M. Pant, and H. Kumar, "Challenges and opportunities in energy transformation during covid-19," *Evergreen*, **8** (*2*) 255–261 (2021). doi:10.5109/4480701.
5) L. Suryanti, S.E.I. Suryani, Hartatiek, Nasikhudin, J. Utomo, A. Taufiq, R. Suryana, Z. Aspanut, and M. Diantoro, "The effect of mn2o3 nanoparticles on its specific capacitance of symmetric supercapacitors fc-zno-x(mn2o3)," *Materials Today: Proceedings*, **44** 3355–3360 (2021). doi:10.1016/j.matpr.2020.11.647.
6) F.U. Zuhri, M. Diantoro, L. Suryanti, T. Suprayogi, Nasikhudin, Sunaryono, and W. Meevasana, "ZnO-fc-nico mof for prospective supercapacitor materials," *Materials Today: Proceedings*, **44** 3385–3389 (2021). doi:10.1016/j.matpr.2020.11.853.
7) B. Priyono, B. Rifky, F. Zahara, and A. Subhan, "Enhancing performance of li4ti5o12 with addition of activated carbon from recycled pet waste as anode battery additives," *Evergreen*, **9** (*2*) 563–570 (2022). doi:10.5109/4794188.
8) M. Nizam, Mufti Reza Aulia Putra, and Inayati, "Heat management on lifepo4 battery pack for eddy current brake energy storage on rapid braking processes," *Evergreen*, **9** (*2*) 451–456 (2022). doi:10.5109/4794171.
9) Anisa Raditya Nurohmah, M. Ayuningtyas, Cornelius Satria Yudha, A. Purwanto, and H. Widiyandari, "Synthesis and characterization of nmc622 cathode material modified by various cheap and abundant transition metals for li-ion batteries," *Evergreen*, **9** (*2*) 427–437 (2022). doi:10.5109/4794168.
10) L. Li, J. Chen, H. Gao, F. Liu, Z. Li, Q. Li, and J. Zhang, "Hierarchical sandwich nife layered double hydroxide/reduced graphene oxide for high energy density asymmetric supercapacitors," *Journal of Electroanalytical Chemistry*, **907** 116065 (2022). doi:10.1016/j.jelechem.2022.116065.
11) T. Kim, E. Samuel, C. Park, A. Aldalbahi, M. El-Newehy, Y. Kang, H.-S. Lee, and S.S. Yoon, "Iron oxide supercapacitor of high volumetric energy and power density using binder-free supersonic spraying and self-healing rgo," *Ceramics International*, **48** (*10*) 13684–13694 (2022). doi:10.1016/j.ceramint.2022.01.250.
12) J. Vigneshwaran, S. Abraham, B. Muniyandi, T. Prasankumar, J.-T. Li, and S. Jose, "Fe2O3 decorated graphene oxide/polypyrrole matrix for high energy density flexible supercapacitor," *Surfaces and Interfaces*, **27** 101572 (2021). doi:10.1016/j.surfin.2021.101572.
13) M. Khairy, K.G. Mahmoud, F.A. Rashwan, H.M. El-Sagher, and C.E. Banks, "Nanosized nickel hexacyanoferrate modified screen-printed electrodes as flexible supercabattery platforms: influence of annealing temperatures and supporting electrolytes," *Journal of Energy Storage*, **46** 103872 (2022). doi:10.1016/j.est.2021.103872.
14) A. Shameem, V. Siva, A. Murugan, M. Mayakkannan, P. Karthikeyan, S. Asath Bahadur, P. Devendran, and A.G. Al-Sehemi, "Synthesis of transition metal oxide-based nanocomposite as a robust electrode with a simple approach for supercabattery application,"

*Journal of Alloys and Compounds*, **979** 173455 (2024). doi:10.1016/j.jallcom.2024.173455.
15) "High-performance supercabattery based on reduced graphene oxide/metal organic framework nanocomposite decorated with palladium nanoparticles - sciencedirect," (n.d.). https://www.sciencedirect.com/science/article/abs/pii/S0013468622003085 (accessed May 15, 2024).
16) M.P. Harikrishnan, A.J.C. Mary, and A.C. Bose, "Electrochemical performance of anio3 (a= la, ce) perovskite oxide material and its device performance for supercapattery application," *Electrochimica Acta*, **362** 137095 (2020). doi:10.1016/j.electacta.2020.137095.
17) H. Tong, D. Gong, J. Liu, J. Xiao, X. Chen, Y. Wu, Y. Zhou, L. Shen, and X. Zhang, "High-performance 2.5 v supercapacitor with high energy density and long cycling stability based on graphene coated oxygen-vacancy birnessite," *Journal of Alloys and Compounds*, **901** 163543 (2022). doi:10.1016/j.jallcom.2021.163543.
18) Y. Gu, W. Du, X. Liu, R. Gao, Y. Liu, H. Ma, J. Xu, and S. Wei, "Matching design of high-performance electrode materials with different energy-storage mechanism suitable for flexible hybrid supercapacitors," *Journal of Alloys and Compounds*, **844** 156196 (2020). doi:10.1016/j.jallcom.2020.156196.
19) S. Anand, M.W. Ahmad, A.K. Ali Al Saidi, D.-J. Yang, and A. Choudhury, "Polyaniline nanofiber decorated carbon nanofiber hybrid mat for flexible electrochemical supercapacitor," *Materials Chemistry and Physics*, **254** 123480 (2020). doi:10.1016/j.matchemphys.2020.123480.
20) Y. Li, P. Kamdem, and X.-J. Jin, "Hierarchical architecture of mxene/pani hybrid electrode for advanced asymmetric supercapacitors," *Journal of Alloys and Compounds*, **850** 156608 (2021). doi:10.1016/j.jallcom.2020.156608.
21) M. Athika, A. Prasath, A.S. Sharma, V.S. Devi, E. Duraisamy, and P. Elumalai, "Ni/nife $_2$ o $_4$ @carbon nanocomposite involving synergistic effect for high-energy density and high-power density supercapattery," *Mater. Res. Express*, **6** (*9*) 095503 (2019). doi:10.1088/2053-1591/ab2c59.
22) K.O. Oyedotun, M.J. Madito, D.Y. Momodu, A.A. Mirghni, T.M. Masikhwa, and N. Manyala, "Synthesis of ternary nico-mno2 nanocomposite and its application as a novel high energy supercapattery device," *Chemical Engineering Journal*, **335** 416–433 (2018). doi:10.1016/j.cej.2017.10.169.
23) H. Yu, H. Xia, J. Zhang, J. He, S. Guo, and Q. Xu, "Fabrication of fe-doped co-mof with mesoporous structure for the optimization of supercapacitor performances," *Chinese Chemical Letters*, **29** (*6*) 834–836 (2018). doi:10.1016/j.cclet.2018.04.008.
24) G.-H. An, "Ultrafast long-life zinc-ion hybrid supercapacitors constructed from mesoporous structured activated carbon," *Applied Surface Science*, **530** 147220 (2020). doi:10.1016/j.apsusc.2020.147220.
25) H. Widiyandari, Oki Ade Putra, R. Suryana, and I. Firdaus, "Highly porous and thermally stable poly(vinylidene fluoride) separators : effects of solvent and colloidal sio_2 concentration," *Evergreen*, **9** (*2*) 443–450 (2022). doi:10.5109/4794170.
26) M.Z. Iqbal, M.M. Faisal, S.R. Ali, and M. Alzaid, "A facile approach to investigate the charge storage mechanism of mof/pani based supercapattery devices," *Solid State Ionics*, **354** 115411 (2020). doi:10.1016/j.ssi.2020.115411.
27) R. Wang, J. Wang, S. Chen, Q. Yuan, D. Li, X. Zhang, L. Chen, Y. Su, G. Tan, and F. Wu, "Effectively stabilizing electrode/electrolyte interface of high-energy lini0.9co0.1o2//si–c system by simple cathode surface-coating," *Nano Energy*, **76** 105065 (2020). doi:10.1016/j.nanoen.2020.105065.
28) J. He, C. Das, F. Yang, and J. Maibach, "Crosslinked poly(acrylic acid) enhances adhesion and electrochemical performance of si anodes in li-ion batteries," *Electrochimica Acta*, **411** 140038 (2022). doi:10.1016/j.electacta.2022.140038.
29) W.-F. Ren, Y. Zhou, J.-T. Li, L. Huang, and S.-G. Sun, "Si anode for next-generation lithium-ion battery," *Current Opinion in Electrochemistry*, **18** 46–54 (2019). doi:10.1016/j.coelec.2019.09.006.
30) Y. Yang, S. Wu, Y. Zhang, C. Liu, X. Wei, D. Luo, and Z. Lin, "Towards efficient binders for silicon based lithium-ion battery anodes," *Chemical Engineering Journal*, **406** 126807 (2021). doi:10.1016/j.cej.2020.126807.
31) B. Xu, P. Zhang, Q. Zhu, Z. Guan, and N. Sun, "Flexible si@c electrode with excellent stability employing mxene as a multi-functional binder for lithium ion batteries," 9 (n.d.).
32) Y. Guo, Y. Wang, Y. Zhang, Y. Zhai, and W. Cai, "Functional sulfur-doped zinc-nickel-cobalt oxide nanorods materials with high energy density for asymmetric supercapacitors," *Journal of Alloys and Compounds*, **896** 163053 (2022). doi:10.1016/j.jallcom.2021.163053.
33) M. Diantoro, A.A. Ittikhad, T. Suprayogi, Nasikhudin, and J. Utomo, "Performance of b-doped srtio$_3$/ ni sheet for supercapacitor material application," *KEM*, **851** 25–31 (2020). doi:10.4028/www.scientific.net/KEM.851.25.
34) S. Di, L. Gong, and B. Zhou, "Precipitated synthesis of al2o3-zno nanorod for high-performance symmetrical supercapacitors," *Materials Chemistry and Physics*, **253** 123289 (2020). doi:10.1016/j.matchemphys.2020.123289.
35) E. Azizi, J. Arjomandi, A. Salimi, and J.Y. Lee, "Fabrication of an asymmetric supercapacitor based on reduced graphene oxide/polyindole/ $\gamma$ − al2o3

ternary nanocomposite with high-performance capacitive behavior," *Polymer*, **195** 122429 (2020). doi:10.1016/j.polymer.2020.122429.
36) M. Liu, K. Turcheniuk, W. Fu, Y. Yang, M. Liu, and G. Yushin, "Scalable, safe, high-rate supercapacitor separators based on the al2o3 nanowire polyvinyl butyral nonwoven membranes," *Nano Energy*, **71** 104627 (2020). doi:10.1016/j.nanoen.2020.104627.
37) N. Talib, Nor Athira Jamaluddin, Tan Kai Sheng, Lee Woon Kiow, H. Abdullah, S. Ahmad, and A. Saleh, "Tribological study of activated carbon nanoparticle in nonedible nanofluid for machining application," *Evergreen*, **8** (*2*) 454–460 (2021). doi:10.5109/4480728.
38) Monica Niken Aprilliani, B. Rusdiarso, and W. Trisunaryanti, "Synthesis of activated carbon-fe_3o_4 composite as gasoline adsorbent in gasoline-water mixture and its adsorption kinetics study," *Evergreen*, **9** (*3*) 701–710 (2022). doi:10.5109/4843101.
39) F. Taufany, Mathilda Jowito Pasaribu, Berlina Yunita Sari Romaji, Y. Rahmawati, A. Altway, Susianto, S. Nurkhamidah, Julfikar Gilang Anfias, Y. Mursidah, F. Desi, S. Yulianti, D. Rahmawati, and G. Stellarosari, "The synthesis of activated carbon from waste tyre as fuel cell catalyst support," *Evergreen*, **9** (*2*) 412–420 (2022). doi:10.5109/4794166.
40) M.M. Ndipingwi, C.O. Ikpo, N.W. Hlongwa, Z. Myalo, N. Ross, M. Masikini, S.V. John, P.G. Baker, W.D. Roos, and E.I. Iwuoha, "Orthorhombic nanostructured li $_2$ mnsio $_4$ /al $_2$ o $_3$ supercapattery electrode with efficient lithium-ion migratory pathway," *Batteries & Supercaps*, **1** (*6*) 223–235 (2018). doi:10.1002/batt.201800045.
41) S. Sivakumar, and L. Nelson Prabu, "Synthesis and characterization of α-mno2 nanoparticles for supercapacitor application," *Materials Today: Proceedings*, **47** 52–55 (2021). doi:10.1016/j.matpr.2021.03.528.
42) W. Sun, Y. Zhang, and F. Yang, "A high-performance symmetric supercapacitor from porous activated carbon under compression," *Energy Tech*, **9** (*5*) 2100068 (2021). doi:10.1002/ente.202100068.
43) G. Yang, and S.-J. Park, "Nanoflower-like nico2o4 grown on biomass carbon coated nickel foam for asymmetric supercapacitor," *Journal of Alloys and Compounds*, **835** 155270 (2020). doi:10.1016/j.jallcom.2020.155270.
44) G. Nagaraju, S.C. Sekhar, B. Ramulu, Sk.K. Hussain, D. Narsimulu, and J.S. Yu, "Ternary mof-based redox active sites enabled 3d-on-2d nanoarchitectured battery-type electrodes for high-energy-density supercapatteries," *Nano-Micro Lett.*, **13** (*1*) 17 (2021). doi:10.1007/s40820-020-00528-9.
45) A. Ahmad, D. Jini, M. Aravind, C. Parvathiraja, R. Ali, M.Z. Kiyani, and A. Alothman, "A novel study on synthesis of egg shell based activated carbon for degradation of methylene blue via photocatalysis," *Arabian Journal of Chemistry*, **13** (*12*) 8717–8722 (2020). doi:10.1016/j.arabjc.2020.10.002.
46) Q. Wei, Z. Chen, Y. Cheng, X. Wang, X. Yang, and Z. Wang, "Preparation and electrochemical performance of orange peel based-activated carbons activated by different activators," *Colloids and Surfaces A: Physicochemical and Engineering Aspects*, **574** 221–227 (2019). doi:10.1016/j.colsurfa.2019.04.065.
47) A. Zhu, H. Xing, Q. Fan, X. Ji, and P. Yang, "Conductive polyaniline coated on aluminum substrate as bi-functional materials with high-performance microwave absorption and low infrared emissivity," *Synthetic Metals*, **271** 116640 (2021). doi:10.1016/j.synthmet.2020.116640.
48) P. Nie, Z. Le, G. Chen, D. Liu, X. Liu, H.B. Wu, P. Xu, X. Li, F. Liu, L. Chang, X. Zhang, and Y. Lu, "Graphene caging silicon particles for high-performance lithium-ion batteries," *Small*, **14** (*25*) 1800635 (2018). doi:10.1002/smll.201800635.
49) F. Zhang, Z. Jia, C. Wang, A. Feng, K. Wang, T. Hou, J. Liu, Y. Zhang, and G. Wu, "Sandwich-like silicon/ti3c2tx mxene composite by electrostatic self-assembly for high performance lithium ion battery," *Energy*, **195** 117047 (2020). doi:10.1016/j.energy.2020.117047.
50) A.F. Bonilla, and D.A. Bonilla, "Production and characterization of a novel lignin-based biopolymer from *Ulex europaeus*," organic chemistry, 2020. doi:10.3762/bxiv.2020.127.v1.
51) A.T. Al-Douri, A.S. Ibraheam, R. Gdoura, Y. Al-Douri, and A.F. Abd El-Rehim, "Morphological and optical investigations of the niznfe $_2$ o $_3$ quaternary alloy nanostructures for potential application in optoelectronics," *Journal of Taibah University for Science*, **15** (*1*) 275–281 (2021). doi:10.1080/16583655.2021.1978834.
52) H. Doloking, A.T. Sartika, and N. Tahar, "Formation of hydrochlorothiazide – para-aminobenzoic acid cocrystals by solvent evaporation method," *Ad-Dawaa.j.Pharm.Sci*, **4** (*1*) (2021). doi:10.24252/djps.v4i1.21301.
53) Firsoni, S.N. Wahyu Hardani, and T. Wahyono, "Fiber content and relative feed value estimation of gamma irradiated rice straw," *IOP Conf. Ser.: Mater. Sci. Eng.*, **546** (*4*) 042008 (2019). doi:10.1088/1757-899X/546/4/042008.
54) K.R. Thorat, and R.B. Laware, "Formulation and evaluation of lornoxicam loaded lyotropic liquid crystalline gel," *J. Drug Delivery Ther.*, **9** (*6*) 116–125 (2019). doi:10.22270/jddt.v9i6.3702.
55) N. Hindryawati, A.S. Panggabean, D.J.N. Subagyono, R.A. Putri, P. Kusmiaty, and G.P. Maniam, "Modification of spent bleaching earth with wo3 and the application for photocatalytic degradation of waste dyestuff under solar light," *JBAT*, **8** (*2*) 84–89 (2020). doi:10.15294/jbat.v8i2.22023.

56) S. Perangin-angin, D. Surbakti, and J.P. Siahaan, "Synthesis of 4-alil-6- (hydroxymethyl) -2-methody phenol compounds from eugenol through mannich reaction followed methylation with methyl iodide and substitution using naoh," **01** (*01*) 11 (2019).
57) P.E. Yuwita, K.W. Mas'udah, Sunaryono, and A. Taufiq, "Structural, morphological, and functional group analysis of corncob powder," in: Malang, Indonesia, 2020: p. 040012. doi:10.1063/5.0015676.
58) X. Bai, H. Zhang, J. Lin, and G. Zhang, "UV-ozone contributions towards facile self-assembly and high performance of silicon-carbon fiber materials as lithium-ion battery anodes," *Journal of Colloid and Interface Science*, **598** 339–347 (2021). doi:10.1016/j.jcis.2021.04.044.
59) A.S. Kamenetskikh, N.V. Gavrilov, P.V. Tretnikov, A.V. Chukin, A.I. Men'shakov, and S.O. Cholakh, "Ion-assisted α-al2o3 coating deposition by anodic arc evaporation at 500–550°c," *Russ Phys J*, **63** (*10*) 1797–1803 (2021). doi:10.1007/s11182-021-02236-2.
60) Y. Tian, Y. An, and J. Feng, "Flexible and freestanding silicon/mxene composite papers for high-performance lithium-ion batteries," *ACS Appl. Mater. Interfaces*, **11** (*10*) 10004–10011 (2019). doi:10.1021/acsami.8b21893.
61) G.Z. Chen, "Supercapattery: merit merge of capacitive and nernstian charge storage mechanisms," *Current Opinion in Electrochemistry*, **21** 358–367 (2020). doi:10.1016/j.coelec.2020.04.002.